

Plasma-Electrolytic-Oxidation Coating containing Y_2O_3 Nanoparticles on AZ91 Magnesium Alloy

Baojun Han^{1,2,*}, Yang Yang^{1,2}, Hao Deng², Yaowu Chen², Chubin Yang^{1,2}

¹ Jiangxi Provincial Engineering Research Center for Magnesium alloys, Gannan Normal University, Ganzhou 341000, China

² School of Chemistry and Chemical Engineering, Gannan Normal University, Ganzhou 341000, China

*E-mail: baojunhan@126.com

Received: 16 February 2018 / Accepted: 12 March 2018 / Published: 10 May 2018

Yttrium oxide (Y_2O_3) nanoparticles were added to the electrolyte during the preparation of a plasma-electrolytic-oxidation (PEO) coating on the AZ91 Mg alloy. The effects of the Y_2O_3 nanoparticles on the microstructure, phase components, chemical compositions, and mechanical properties of the PEO coating were investigated by scanning electron microscopy (SEM), energy dispersive spectroscopy (EDS), X-ray diffraction (XRD), and microhardness tests. Furthermore, the corrosion resistance of the PEO coating was evaluated by potentiodynamic polarization curves and electrochemical impedance spectroscopy (EIS). The results indicated that the Y_2O_3 nanoparticles had been incorporated into the PEO coating and that the number of micropores and cracks in the coating was dramatically decreased. The microhardness of the PEO coating was more than 10 times higher than that of the AZ91 Mg substrate, and the corrosion current density decreased by approximately three orders of magnitude when 3 g/L of Y_2O_3 nanoparticles was added to the corresponding electrolyte.

Keywords: AZ91 Mg alloy, plasma-electrolytic-oxidation (PEO) coating, Y_2O_3 nanoparticle, corrosion resistance, microhardness

1. INTRODUCTION

Magnesium (Mg) alloys have advantages such as low density, high specific strength, good castability, better thermal conductivity, excellent magnetic shielding, and easy recyclability, which give Mg alloys great potential for application in the aerospace industry, automobile manufacture, and computer, communications, and consumer electronic (3C) electric products [1,2]. However, the high chemical activity and poor corrosion resistance of Mg alloys seriously restrict their extensive application and development [3,4]. The main direct and efficient approach to improve the corrosion resistance of Mg alloys is surface treatment [5]. Several methods have been proposed and used to

improve the surface performance of Mg alloys [6]. Among them, plasma electrolytic oxidation (PEO) was believed to be the most promising prospect because it shows superior properties such as firm bonding strength, stability, ease of operation, and use of environmentally friendly electrolytes [7,8]. During PEO, the coating is formed by material deposition from anodic, thermal, and plasma chemical processes associated with repetitive discharge events to obtain a coating comprised of the components of the Mg alloy substrate and the electrolyte. Hence, it is possible to adjust the performance of PEO coatings by varying the processing conditions and electrolyte components [9-10].

Unfortunately, as reported elsewhere in the literature [11-13], PEO coatings show a significant amount of porosity and numerous cracks, so they cannot provide long-term substrate protection. Over the past few decades, the addition of particles to PEO electrolytes has been explored as strategy for yielding anticorrosive, catalytic, wear-resistant, and other types of functional PEO coatings [14-16]. Nasiri Vatan et al. [17] investigated the microstructural, tribological, and electrochemical properties of the coating containing SiC nanoparticles produced by PEO on the AZ31 Mg alloy. They found that the SiC-containing coating registered a much lower friction coefficient and wear rate than the uncoated AZ31 Mg alloy and the SiC-free coatings. Lu et al. [18] fabricated a photocatalytic active PEO coating on the AM50 Mg alloy by adding TiO₂ particles to the electrolyte, and the results indicated that a lower treatment voltage and a higher concentration of particles in the electrolyte could be used to incorporate more TiO₂ particles into the coating and generate superior photocatalytic and functional coatings. Mashtalyar et al. [19] investigated the formation of protective multifunctional coatings on the MA8 Mg alloy, using PEO in an electrolyte containing titanium nitride nanoparticles and established that the microhardness of the coating containing 3 g/L of nanoparticles had doubled. Stojadinović et al. [20] reported the fabrication of MgO/ZnO photoactive PEO coatings on the AZ31 Mg alloy by adding ZnO particles to the phosphate-based alkaline electrolyte. The results indicated that although the surface morphology of the coating was not significantly influenced by the addition of the ZnO particles, the photoluminescent emission spectra of the MgO/ZnO coatings featured a sharp band centered at about 380 nm and a broad band centered at about 535 nm with the leading contribution coming from the ZnO particles deposited on the surface and that the photoactivity of the obtained coatings increased with increasing processing time and ZnO concentration up to 6 g/L. Lim et al. [21] fabricated PEO coatings on the AZ31 Mg alloy in Na₂SiO₃-based electrolytes containing CeO₂ particles and found that the CeO₂ particles had been incorporated into the coatings at an early stage and were preferentially located in the outer porous layer and filled micropores. Additionally, the corrosion resistance of the AZ31 Mg alloy was significantly improved by the incorporation of the CeO₂.

All the aforementioned reports indicated that the addition of particles to the electrolyte could significantly improve the mechanical and corrosion-resistant performances of the PEO coatings. To the best of our knowledge, there have been no report to date about using yttrium oxide (Y₂O₃) as an electrolyte component for producing PEO coatings. The melting point of Y₂O₃ is about 2410°C, and Y₂O₃ shows high hardness and excellent corrosion resistance, which make it a good candidate material for maintaining high resistance to harsh plasma etching environments and for exhibiting superior plasma and chemical resistance against etching by Cl⁻, F⁻, and O²⁻, all of which easily etch Mg alloys [22-24].

The aim of the present investigation was to explore the microstructure and surface performance of the PEO coatings on the AZ91 Mg alloy processed in silicate electrolyte containing Y_2O_3 nanoparticles. The surface morphology, chemical composition, and phase components of the PEO coating were characterized by scanning electron microscopy (SEM), energy disperse spectroscopy (EDS), and X-ray diffraction (XRD). The corrosion resistance and mechanical properties of the PEO coating containing the Y_2O_3 nanoparticles were also evaluated using an electrochemical test station and a microhardness tester.

2. EXPERIMENTAL

2.1 Materials and methods

A commercial AZ91 Mg alloy was utilized as the substrate material for the PEO experiments in the present investigation. The chemical composition of the AZ91 Mg alloy is listed in Table 1.

Table 1. Chemical composition of the AZ91 Mg alloy.

Element	Al	Zn	Mn	Si	Fe	Cu	Mg
Content (wt.%)	8.95	0.93	0.21	0.011	0.08	0.01	Balance

The samples were cut into 10 mm × 10 mm × 10-mm coupons, which were grounded using silicon carbide abrasive papers from 600 up to 1500-grit. Subsequently, the samples were ultrasonically rinsed with acetone and distilled water, air-dried at room temperature, and processed by PEO.

The PEO processing was executed on a 30 kW bipolar pulse power supply (WHD30, Harbin Institute of Technology) equipped with an electrolyte cooling system. The AZ91 samples were used as the anode, and a 316L stainless steel bath was used as the cathode. The electrolytes were maintained in the range 25–35°C and were persistently stirred by compressed air during the PEO processing.

The processing electrolytes used in the present investigation consisted of 20 g/L of $Na_2SiO_3 \cdot 10H_2O$, 4 g/L of KOH, 2 g/L of $Na_5P_3O_{10}$, 10 ml/L of glycerol, and 0, 1, 3, or 5 g/L of Y_2O_3 nanoparticles, respectively. Unless otherwise stated, all the chemical reagents were analytical reagent (AR) grade. The Y_2O_3 nanoparticles were about 40 nm in diameter and were purchased from the Aladdin Company, China. The electrolytes were ultrasonically dispersed for 30 min to homogeneously suspend the Y_2O_3 nanoparticles prior to the PEO processing.

Based on many trials under different conditions, the PEO processing parameters used in the present investigation are listed in Table 2. The PEO-processed samples subsequently were washed in ethanol and distilled water and were air-dried at room temperature.

Table 2. PEO processing parameters used in present investigation.

processing parameters	positive voltage	negative voltage	processing frequency	duty cycle	duty ratio	processing time
value	450 V	30 V	800 Hz	10%	1:1	20 min

2.2 Coating characterization

The thickness of the PEO coatings was measured using a digital thickness gauge (Time, TT230), and the average of 10 point measurements was reported. The micro-hardness of the coatings was tested using a micro-hardness tester (Shimadzu, HMV-21GST) with a load of 500 g and a holding time 50 s, and the average of 5 point measurements was used in the present work. The surface and cross-sectional morphologies of the coatings were observed by scanning electron microscopy (SEM, Quanta, FEI450). The chemical compositions of the coatings were analyzed by energy dispersive spectroscopy (EDS, Oxford) attached to the SEM. The phase components of the coatings were identified by X-ray diffraction (XRD, Bruker, D8 ADVANCE) with Cu K α radiation ($\lambda = 0.154060$ nm) over $2\theta = 10\text{--}90^\circ$. The zeta potential of the Y₂O₃ nanoparticles was measured by Zetasizer Nano ZS (Malvern, USA).

The corrosion resistances of the coatings were evaluated by the potentiodynamic polarization curves and by electrochemical impedance spectroscopy (EIS) measurements in a 3.5% NaCl solution, using an electrochemical workstation (Metrohm, PGSTA302A) equipped with a three-electrode cell comprised of reference (saturated calomel), counter (platinum foil) and working (sample) electrodes. The area of the working electrode was 1.0 cm². All the electrochemical tests were conducted on cells immersed for 30 min in the 3.5 wt.% NaCl solution at room temperature to attain a steady state of the open circuit potential (OCP), whereas at least three independent measurements were performed under each experimental condition. The EIS measurements were executed at OCP in the range 10⁻²–10⁵ Hz. The dynamic polarization curves were scanned at 1 mV/s from -0.2 to 0.3 V with respect to the OCP. The electrochemical parameters such as the corrosion potential (E_{corr}) and corrosion current density (i_{corr}) were derived by the Tafel extrapolation method according to the achieved dynamic polarization curves [25,26].

3. RESULTS AND DISCUSSION

3.1 Current versus processing time curves

Fig.1 shows the variation of current with processing time under constant voltage for the samples with different concentrations of Y₂O₃ nanoparticles addition. Clearly, the curves for all the PEO-coated samples showed almost identical shapes, i.e., as the PEO processing proceeded, the current sharply decreased and then gradually decreased to about zero with increasing time, which is similar to the results of previous studies [27-29]. Although three characteristic stages can be identified from the curves, sparks could not be observed during PEO processing owing to the opacity of the

electrolytes. During the first stage (about 0–100 s), the current decreased almost linearly with time, corresponding to conventional anodizing processing. During the second stage (about 100–600 s), the slopes of the curves decreased, corresponding to the formation of a non-uniform PEO coating. The formation of a PEO coating will increase the electrical resistance and decrease the current. During the third stage (about 600–1200 s), the slope was approximately zero because a compact, uniform coating with a large electrical resistance was formed and had grown. Furthermore, Fig. 1 also shows that although the addition of Y_2O_3 nanoparticles did not noticeably affect the three-stage characteristic evolution of the current versus processing-time curves throughout the PEO process, the samples containing the Y_2O_3 nanoparticles needed more time to reach the second stage, and their final current was slightly reduced. Similar results have been reported elsewhere in the literature [30].

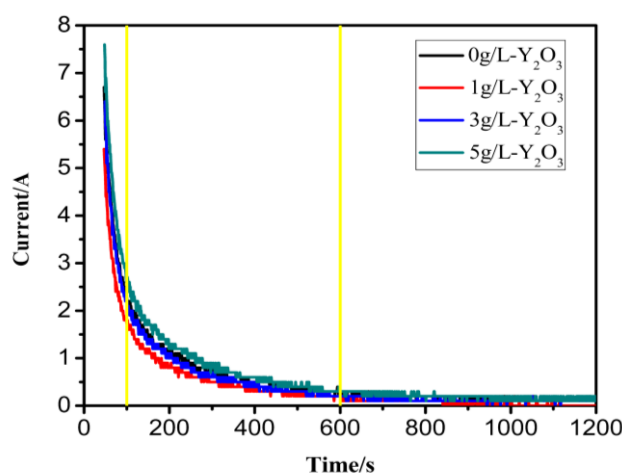


Figure 1. The variation of current with processing time for the samples processed by PEO in electrolytes containing different concentrations of Y_2O_3 nanoparticles

3.2 Thickness and micro-hardness

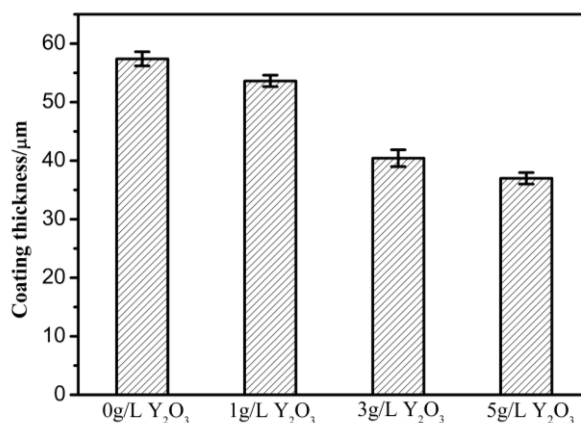


Figure 2. Thicknesses of the PEO coatings processed in electrolytes containing different concentrations of Y_2O_3 nanoparticles

Fig. 2 shows the coating thicknesses of the different samples. It is evident that with the introduction of Y_2O_3 nanoparticles, the PEO coatings became thinner and that the coating thickness decreased with increasing Y_2O_3 nanoparticle content. The PEO coating containing 5 g/L of Y_2O_3 nanoparticles was the thinnest. A similar result has been reported by Lu et al. [31-33], t found that the growth rates of coatings were reduced by the addition of particles such as SiO_2 , WC, Si_3N_4 , etc.

Fig. 3 shows the micro-hardness of the AZ91 Mg alloy substrate and those of the PEO samples processed in electrolytes with and without Y_2O_3 nanoparticles. Clearly, PEO processing improved the micro-hardness of the substrate. The micro-hardness of the AZ91 Mg alloy substrate was only about 52 HV and that of the PEO coating processed without any Y_2O_3 nanoparticles was 423 HV. Further, the addition of the Y_2O_3 nanoparticles increased the micro-hardness of the PEO coatings. Among the PEO coatings processed in the electrolytes containing the Y_2O_3 nanoparticles, the PEO coating processed with 3 g/L of Y_2O_3 nanoparticles showed the highest micro-hardness—reaching about 583 HV, more than 10 times higher than that of the substrate. The increased micro-hardness of the PEO coatings processed in the electrolytes with the Y_2O_3 nanoparticles is attributed to their higher density; they are much denser than the PEO coating processed in the electrolyte without any Y_2O_3 nanoparticles. Furthermore, the micro-hardness measurements of the PEO coating processed in the electrolyte with 3 g/L of Y_2O_3 nanoparticles displayed the lowest standard deviation among all the micro-hardness measurements, illustrating the uniformity of that particular coating.

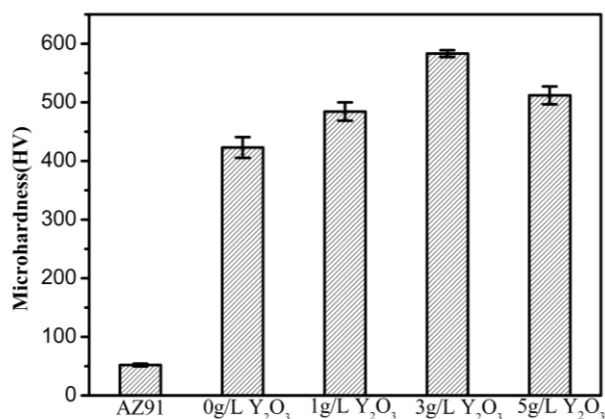


Figure 3. Micro-hardness of the AZ91 substrate and the PEO coatings processed in electrolytes containing different concentrations of Y_2O_3 nanoparticles

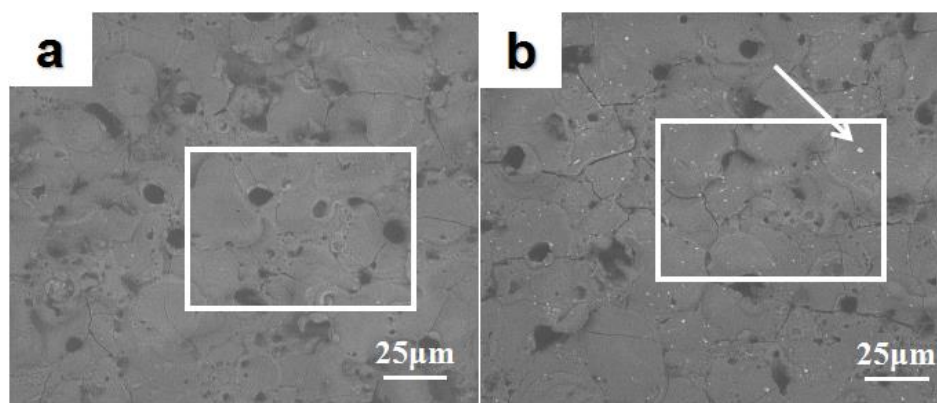
3.3 Surface morphologies and phase compositions

Fig. 4 shows the SEM surface morphologies of the PEO coatings obtained in the electrolytes without and with different contents of Y_2O_3 nanoparticles. Clearly, the addition of the Y_2O_3 nanoparticles did not significantly change the surface morphology of the coatings, i.e., all the coatings displayed similar surface morphology features, and some micro-pores and cracks were embedded in the PEO coatings, which is typical of the surface morphology of PEO coatings and has been reported in numerous corresponding studies [34,35]. The micro-pores were formed by the extraction of the molten oxide and gas bubbles from the micro-discharge channels, and the cracks were formed by the

thermal stress due to the rapid solidification of the molten oxide in the relatively cool electrolyte [34-36]. The lower Pilling-Bedworth ratio (PBR) of magnesium is another reason for the high porosity of PEO coatings on Mg alloys [37]. Fig. 4 also reveals the differences in the surface morphologies of the PEO coatings obtained in electrolytes without and with different contents of Y_2O_3 nanoparticles. The surface morphologies of the PEO coatings obtained in the electrolytes with different contents of Y_2O_3 nanoparticles show some tiny specks of a white substance adhering to the coating surface, as indicated by the arrows in Fig. 4, whereas the surface morphology of the PEO coating obtained in the electrolyte without any Y_2O_3 nanoparticles does not. These results indicate that the Y_2O_3 nanoparticles may have participated in the growth of the PEO coating. In order to determine whether they did, the chemical compositions of the coatings were analyzed by EDS, and the results are summarized in Table 3. The PEO coating processed in the electrolyte without any Y_2O_3 nanoparticles mainly contained Mg, O, Si, and Al, whereas the PEO coatings processed in the electrolytes with Y_2O_3 nanoparticles mainly contained Mg, O, Si, Al, and Y. Clearly, yttrium was identified in the coatings processed in the electrolytes containing the Y_2O_3 nanoparticles. Furthermore, the yttrium concentrations of the PEO coatings prepared in electrolytes containing 0, 1, 3, and 5 g/L of Y_2O_3 nanoparticles were 0, 1.04, 3.47, and 4.25 wt.%, respectively, as determined by EDS. Thus, the concentration of yttrium in the PEO coatings increased with increasing Y_2O_3 nanoparticle concentration in the electrolyte. Fig. 5 displays a magnified morphology of the white substance shown in Fig. 4, and the corresponding results of the EDS chemical composition analysis are listed in Table 4. The white substance emerging on the surfaces of the PEO coatings prepared in the electrolytes containing the Y_2O_3 nanoparticles was mainly composed of Mg, O, and Y, and the ratio of Y was up to 26.17 wt.%, implying that the Y_2O_3 nanoparticles may have participated in the growth of the PEO coatings.

Table 3. EDS chemical composition analysis of the PEO coatings, as indicated by the boxes in Figure 4.

Element Sample	Mg (wt.%)	O (wt.%)	Si (wt.%)	Al (wt.%)	Y (wt.%)
0 g/L Y_2O_3	42.88	38.45	16.22	2.44	0
1 g/L Y_2O_3	36.05	47.39	10.86	4.66	1.04
3 g/L Y_2O_3	29.95	54.35	11.17	1.06	3.47
5 g/L Y_2O_3	32.17	49.17	13.61	0.80	4.25



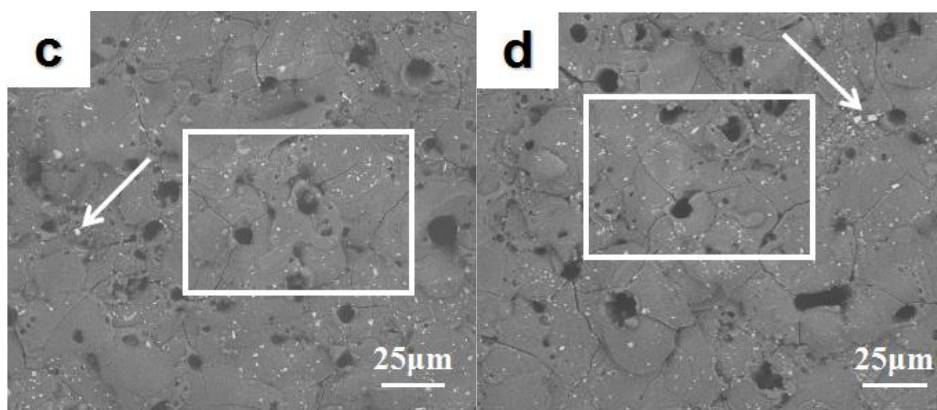


Figure 4. SEM surface morphologies of the PEO coatings obtained in the electrolytes (a) without and with (b) 1, (c) 3, and (d) 5 g/L of Y_2O_3 nanoparticles.

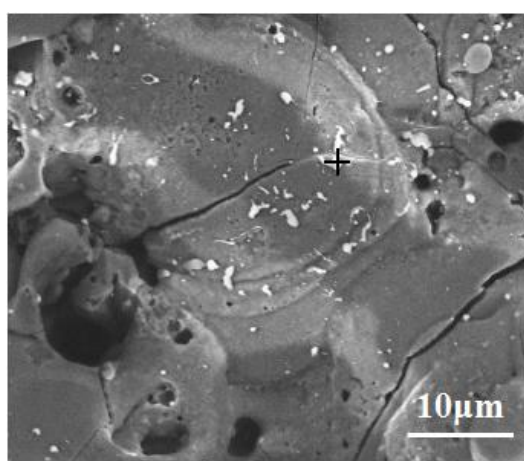


Figure 5. The magnified surface morphology of the white substance shown in Figure 4.

Table 4. The chemical composition of the area indicated in Figure 5, as determined by EDS point scanning.

Element	Mg	O	Si	Al	Y
Content (wt.%)	29.22	36.67	7.61	0.34	26.17

Fig. 6 discloses the cross-sectional morphologies of the PEO coatings prepared in electrolytes without and with Y_2O_3 nanoparticles. Clearly, all the coatings showed two main coating regimes, i.e., outer and inner layers, which is typical of the cross-sectional morphologies of PEO coatings [38-40]. The outer layer shows some micro-pores, and the inner layer is denser than the outer layer. The inner layer of the PEO coating processed in the electrolyte without any Y_2O_3 nanoparticles was thinner than those of the PEO coatings processed in the electrolytes with the Y_2O_3 nanoparticles, and the micro-pores in the outer layer of the former were larger than those in the outer layers of the latter. Further, some of the micro-pores in the outer layer of the former penetrated the inner layer (Fig. 6a). With the introduction of the Y_2O_3 nanoparticles, the inner layer of the PEO coatings became denser and thicker,

and the size and number of micro-pores decreased (Fig. 6b,c). However, when the concentration of Y_2O_3 nanoparticles in the electrolyte was too high, the number of micro-pores increased, and the inner layer became thinner (Fig. 6d). Further, some white particles agglomerated across the entire cross-sections of the PEO coatings prepared in the electrolytes with the Y_2O_3 nanoparticles (Fig. 6b-d). In order to further identify the chemical compositions of the white agglomerates, EDS mapping scanning was conducted on the PEO coating processed in the electrolyte with 3 g/L of Y_2O_3 nanoparticles, and the results are shown in Fig. 7. Mg, O, Si, and Y were the main elements in the coating. Among them, Si and O were relatively uniformly distributed throughout the whole coating. The signal for Mg was weak. At the same time, the signal for Y was inhomogeneously distributed and localized only at certain positions.

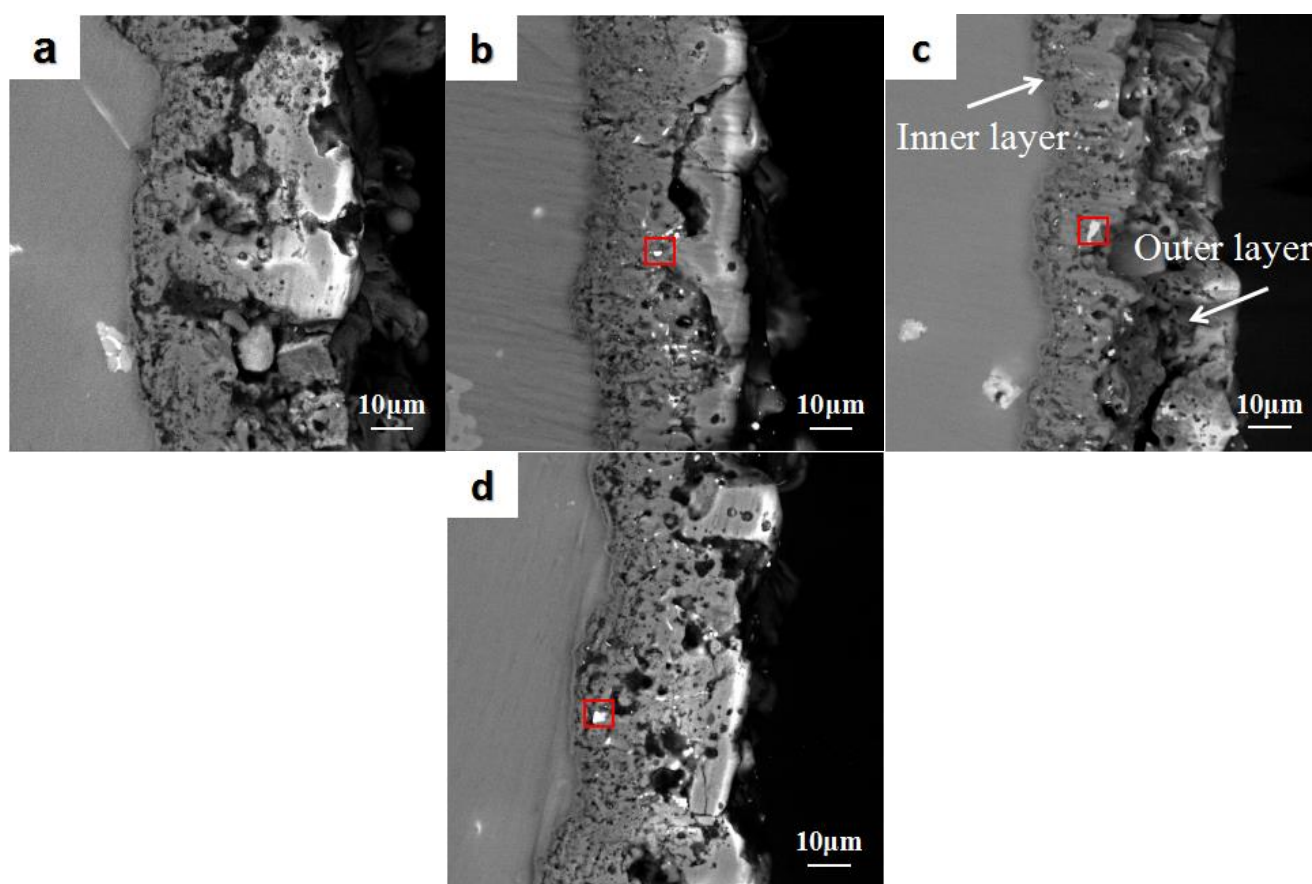


Figure 6. Cross-sectional SEM morphologies of the PEO coatings obtained in electrolytes (a) without and with (b) 1, (c) 3, and (d) 5 g/L of Y_2O_3 nanoparticles.

The detection of yttrium suggests that the Y_2O_3 nanoparticles had been incorporated into the PEO coatings as there was no other yttrium source except for the Y_2O_3 nanoparticles in the electrolytes. Clearly from Figs. 6 and 7, the incorporated particle agglomerates were preferentially located at the margins of the micro-pores because they could enter the coatings more easily and frequently through the open pores and the old discharge channels and through which the Y_2O_3 nanoparticles could heal the imperfections in the PEO coatings. Similar results have been reported

elsewhere in the literature [11, 34, 41]. The reported isoelectric point of Y_2O_3 is pH 9.1 [42], and the zeta potential of the Y_2O_3 nanoparticles was -23.6 mV in the present electrolyte; thus, the negative surface charge of the Y_2O_3 nanoparticles enabled them to easily migrate toward the anode (substrate) where they were incorporated into the PEO coatings in the high electric field during PEO processing. The compressed air used during PEO processing also may have driven the Y_2O_3 nanoparticles in the electrolyte to participate in the formation of the PEO coating. From the analysis, the Y_2O_3 nanoparticles in the electrolyte during PEO processing could be incorporated into the PEO coating, reducing its porosity and helping to obtain a more compact, uniform coating.

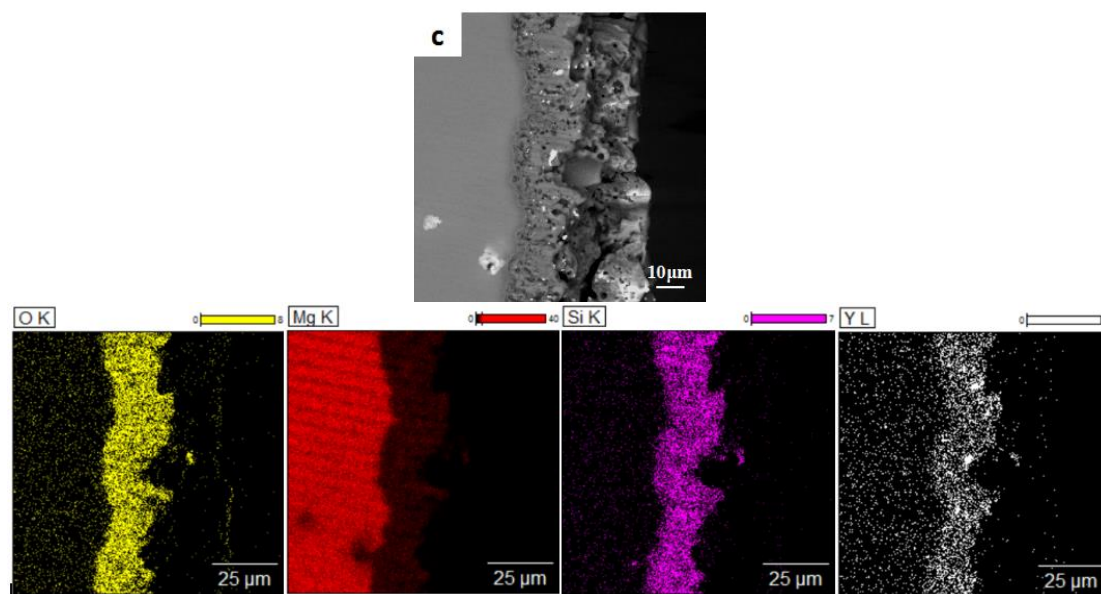
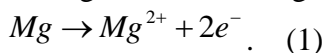
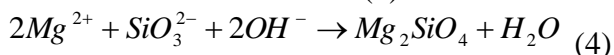
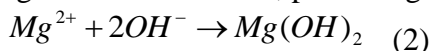


Figure 7. EDS elemental maps of the PEO coatings obtained in the electrolyte with 3 g/L of Y_2O_3 nanoparticles.

The XRD patterns of the PEO coatings prepared in the electrolytes containing different concentrations of Y_2O_3 nanoparticles are shown in Fig. 8. According to the XRD results, the main components of the coating formed on the AZ91 Mg alloy processed in the electrolyte without any Y_2O_3 nanoparticles were phases of Mg, MgO, and Mg_2SiO_4 (Fig. 8a). It should be pointed out that the peaks for the MgO and Mg_2SiO_4 were close to each other in the XRD patterns. The appearance of the Mg peaks in the diffraction patterns for all the coatings was due to the penetration of x-rays through the coatings and the x-ray reflections coming from the substrates. The MgO and Mg_2SiO_4 peaks were from the PEO coatings. The nature of each new phase formed during the PEO processing depends on the chemical composition of the substrate and the corresponding electrolyte. During the PEO process, the Mg alloy substrate was used as the anode; thus, the magnesium dissolved, producing magnesium ions according to the following reaction



Under high applied potentials, the magnesium ions migrated outward away from the anode (i.e., the Mg substrate) into the electrolyte and at the same time, SiO_3^{2-} and OH^- migrated inward from the electrolyte to the anode (i.e., the Mg substrate). The coating formation reactions occurred once the concentrations of the ions at the Mg substrate/electrolyte interface reached certain levels. The following reactions occurred, producing the MgO and Mg_2SiO_4 phases.



It is noteworthy that the signal of Y_2O_3 was also detected in the XRD patterns of the PEO coatings processed in the electrolytes with the Y_2O_3 nanoparticles (Fig. 8 b-d), implying that the Y_2O_3 nanoparticles had been incorporated into the PEO coatings. The XRD analysis results were consistent with the aforementioned EDS analysis results.

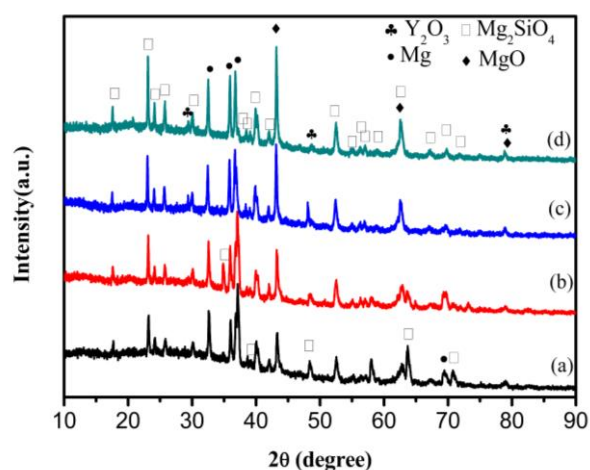


Figure 8. XRD patterns of the PEO coatings obtained in electrolytes (a) without and with (b) 1, (c) 3, and (d) 5 g/L of Y_2O_3 nanoparticles.

3.4 Corrosion resistance

Potentiodynamic polarization and EIS were used to reveal the corrosion resistances of the coatings. The corrosion current density (i_{corr}) and corrosion potential (E_{corr}) are frequently used to evaluate the early stages of corrosion resistance of samples. The anodic polarization curve is the important feature related to the corrosion resistance, while the cathodic polarization curve corresponds to the evolution of hydrogen [43]. Fig. 9 illustrates the potentiodynamic polarization curves of the blank AZ91 Mg alloy and the PEO coatings prepared in the electrolytes containing different concentrations of Y_2O_3 nanoparticles. The electrochemical parameters derived by Tafel extrapolation are summarized in Table 5. Clearly, the PEO coatings can decrease the anodic current density of the AZ91 Mg alloy, indicating that the PEO coatings restrained the anodic reaction and enhanced the electrochemical stability of the AZ91 Mg alloy. The blank AZ91 exhibited the lowest corrosion

potential (E_{corr}) and the highest corrosion current density (i_{corr}), implying that PEO processing can significantly improve the corrosion resistance of the AZ91. Especially, the corrosion current densities of the PEO coatings prepared in the electrolyte containing 3 g/L of Y_2O_3 nanoparticles were up to $1.62 \times 10^{-7} \text{ A/cm}^2$ and were about 3 orders of magnitude lower than that of the blank AZ91 ($1.78 \times 10^{-4} \text{ A/cm}^2$).

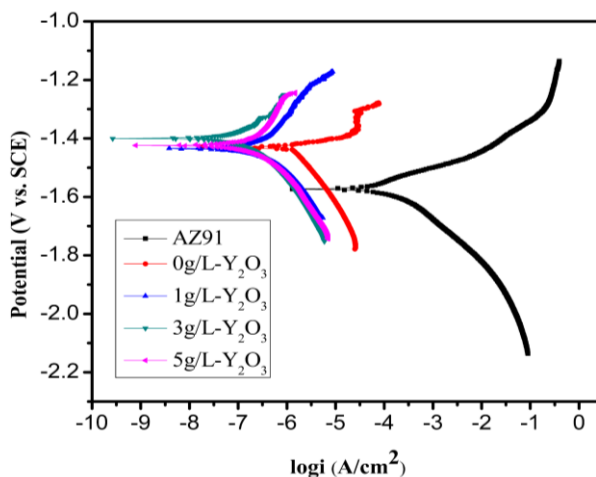


Figure 9. Potentiodynamic polarization curves of the blank AZ91 Mg alloy and the PEO coatings processed in the electrolytes containing different concentrations of Y_2O_3 nanoparticles

Table 5. Electrochemical parameters derived by Tafel extrapolation from the curves in Figure 9

Sample	Electrochemical parameter				
	AZ91	PEO	PEO+ 1 g/L Y_2O_3	PEO+ 3 g/L Y_2O_3	PEO+ 5 g/L Y_2O_3
Corrosion potential (E_{corr}) (V)	-1.57	-1.43	-1.43	-1.40	-1.42
Corrosion current density (i_{corr})(A/cm^2)	1.78×10^{-4}	1.38×10^{-6}	3.72×10^{-7}	1.62×10^{-7}	2.29×10^{-7}

EIS measurements were conducted to determine the long-term corrosion performance of the PEO coatings. Fig. 10 shows the Nyquist plots for the blank AZ91 and the PEO-coated samples processed in the electrolytes containing different concentrations of Y_2O_3 nanoparticles. Fig. 10a shows a capacitive semicircle at the medium and high frequencies and an inductive semicircle at the low frequency in the Nyquist plot for the blank AZ91. The inductive semicircle at the low frequency shows that the blank AZ91 can be easily corroded under harsh conditions, whereas Fig. 10b shows only one capacitive semicircle each at the medium and high frequencies in the Nyquist plots for the PEO coatings, and their capacitive semicircle radii are much larger than that for the blank AZ91 (Fig. 10a).

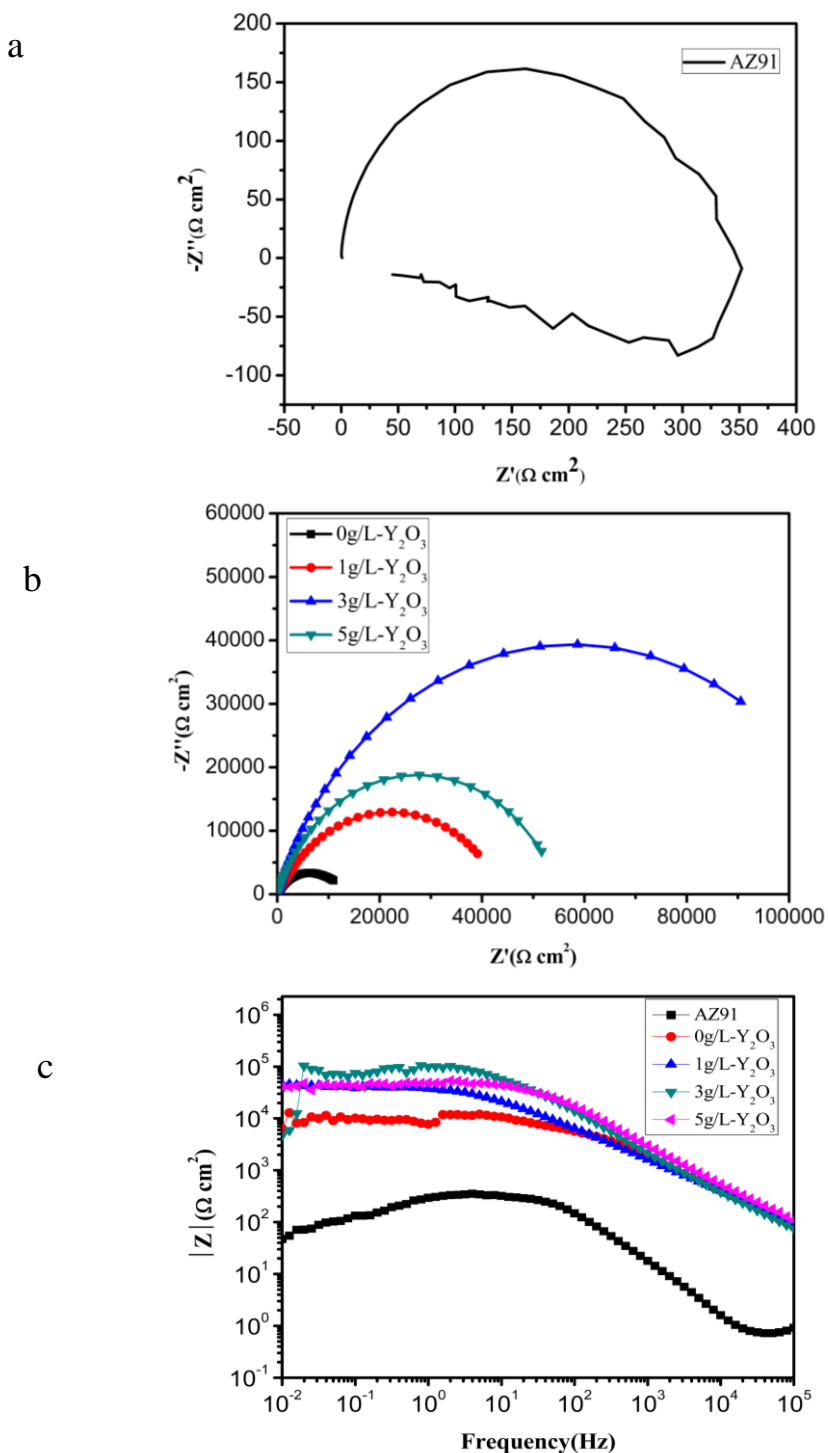


Figure 10. EIS analysis of the blank AZ91 Mg alloy and the PEO coatings. Nyquist plots of (a) the blank AZ91 and (b) the PEO coatings processed in the electrolytes containing different concentrations of Y_2O_3 nanoparticles, and (c) Bode plots for the PEO coatings processed in the electrolytes containing different concentrations of Y_2O_3 nanoparticles.

Furthermore, the capacitive semicircle radius increased with increasing concentration of Y_2O_3 nanoparticles in the electrolyte. Since a larger semicircle radius indicates higher corrosion resistance [44] and since the PEO coating processed in the electrolyte containing 3 g/L of Y_2O_3 nanoparticles had

the largest capacitive semicircle radius, it had the best corrosion resistance. Fig. 10c presents the impedance measurements obtained from the Bode plots for the blank AZ91 and the PEO coatings processed with and without Y_2O_3 nanoparticles in the electrolyte. The analysis of the frequency behavior of the impedance allows for the determination of the corrosion mechanism and the coating robustness [45]. Fig 10c indicates that in the low-frequency range (10^{-2} – 10^0 Hz), the total ($|Z|$) impedance of the blank sample was in the range 10^1 – $10^2 \Omega \text{ cm}^2$ whereas in the same frequency range, the impedances of the PEO coatings were up to $10^5 \Omega \text{ cm}^2$. The impedance at the lower frequency can be used to assess the corrosion resistance of the coating and characterize the inner layer properties [46]. Therefore, the increasing impedance implies the obvious improvement in corrosion resistance.

According to the SEM microstructure observations and the EIS measurements, the impedance spectra for the samples were interpreted by the equivalent circuit, as shown in Fig. 11, in which the R_s , R_1 , and R_2 represent the electrical resistances of the solution, the outer layer, and the inner layer, respectively. The CPE1 and CPE2 are constant phase elements representing the outer and inner layers, respectively. The variation in the equivalent circuit parameters could be utilized to assess the corrosion resistances of the coatings. In Table 6, the values of the equivalent circuit elements are summarized, and n_p is a dispersion effect index close to 1. Clearly, R_1 and R_2 both increased with increasing concentration of Y_2O_3 nanoparticles in the electrolyte. The corrosion resistance of the PEO coatings is mainly determined by the microstructure and performance of inner layer, i.e., the higher the R_2 the higher the corrosion resistance of the PEO coatings [47,48]. Thus, according to the results summarized in Table 6, the PEO coating processed in the electrolyte containing 3 g/L of Y_2O_3 nanoparticles had the best corrosion resistance.

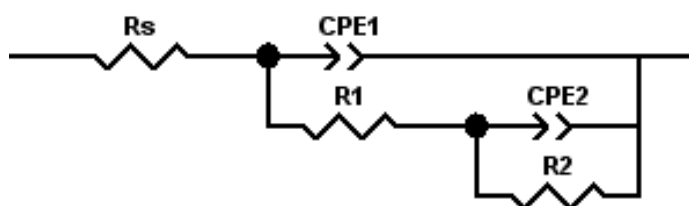


Figure 11. Equivalent circuit used to fit the EIS spectra in the present investigation

Table 6. Electrochemical parameters of the PEO coatings fitted according to the EIS spectra and the equivalent circuit shown in Fig. 11.

	R_s ($\Omega \text{ cm}^2$)	R_1 ($\Omega \text{ cm}^2$)	CPE1-T ($\Omega^{-1} \text{ S}^n \text{ cm}^{-2}$)	CPE1-P (n_t)	R_2 ($\Omega \text{ cm}^2$)	CPE2-T ($\Omega^{-1} \text{ S}^n \text{ cm}^{-2}$)	CPE2-P (n_t)
0 g/L Y_2O_3	18.03	727.7	1.25×10^{-6}	0.68113	17823	1.9388×10^{-5}	0.134063
1 g/L Y_2O_3	28.15	5587	1.625×10^{-6}	0.6659	38615	2.9457×10^{-7}	0.73315
3 g/L Y_2O_3	18.38	36799	4.0088×10^{-7}	0.79452	82227	5.056×10^{-7}	0.46726
5 g/L Y_2O_3	18.19	2500	3.1759×10^{-7}	0.78196	53417	1.7746×10^{-7}	0.45915

The present experimental results demonstrated that the addition of Y_2O_3 nanoparticles to the PEO electrolyte for the AZ91 Mg alloy could significantly improve the mechanical properties and corrosion resistances of the PEO coatings, which can be attributed to the special structures and compositions of the PEO coatings achieved with the incorporation of the Y_2O_3 nanoparticles. During the PEO coating formation, the Y_2O_3 nanoparticles could be embedded into the outer and inner layers of the coatings, especially into the inner layers, causing the inner layers of the coatings to become significantly more compact and thicker because the Y_2O_3 nanoparticles were preferentially located at the micro-pores and cracks of the coatings. When the coated samples were immersed in the corrosion medium, the Y_2O_3 nanoparticles prevented the corrosion medium from penetrating the inner layers, thereby improving the corrosion resistance of the Mg substrate.

4. CONCLUSIONS

In the present investigation, Y_2O_3 nanoparticles were added to the electrolyte used during PEO processing to reduce the number of micro-pores in and improve the surface performance of PEO coatings on the AZ91 Mg alloy. The microstructural and chemical composition investigations indicated that the Y_2O_3 nanoparticles were incorporated into the PEO coatings and that they dramatically decreased the number of micro-pores in the PEO coatings. The electrochemical measurements and the results of the mechanical performance tests demonstrated that the incorporation of the Y_2O_3 nanoparticles into the PEO coatings significantly improved the surface performance of the coatings. The micro-hardness of the PEO coating was increased to more than 10 times that of the blank AZ91 Mg alloy and the corrosion current of the PEO coating was decreased by approximately three orders of magnitude compared with that of the blank AZ91 when 3 g/L of Y_2O_3 nanoparticles was added to the electrolyte. The addition of higher concentrations of Y_2O_3 nanoparticles to the electrolyte increased the number of micro-pores and decreased the uniformity of the coating structures, resulting in decreased mechanical strength and corrosion resistance.

ACKNOWLEDGEMENTS

The authors acknowledge the support of the Ground Plan of Science and Technology Projects of Jiangxi Province (Grant No. KJLD2013078), the Open Project of the Jiangxi Provincial Engineering Research Center for Magnesium Alloys (Grant No. 2017), and the Innovation and Entrepreneurship Training Program for College Students of Gannan Normal University (Grant No. 201766).

References

1. B.L. Mordike and T. Ebert, *Mater. Sci. Eng. A*, 302 (2001) 37.
2. A. Apelfeld, B. Krit, V. Ludin, N. Morozova, B. Vladimirov and R.Z. Wu, *Surf. Coat. Technol.*, 322 (2017) 127.
3. L.J. Liu and M. Schlesinger, *Corros. Sci.*, 51 (2009) 1733.
4. X.J. Cui, M.T. Li, R.S. Song and Z.X. Yu, *Appl. Surf. Sci.*, 363 (2016) 91.
5. J. Tang and K. Azumi, *Electrochim. Acta*, 56 (2011) 8776.

6. S. Bender and J. Göllner, *Fundamentals of Magnesium Alloy Metallurgy*, Woodhead Publishing, (2013) 232.
7. M. Daroonparvar, M.A.M. Yajid, N.M. Yusof and H.R. Bakhsheshi-Rad, *J. Alloys Compd.*, 688 (2016) 841.
8. Z.P. Yao, P.F. Ju, Q.X. Xia, J.K. Wang, P. Su, H. Wei, D.Q. Li and Z.H. Jiang, *Surf. Coat. Technol.*, 307 (2016) 1236.
9. S.V. Gnedenkov, S.L. Sinebryukhov, D.V. Mashtalyar and I.M. Imshinetskiy, *Surf. Coat. Technol.*, 283 (2015) 347.
10. V. shoaie-Rad, M.R. Bayati, H.R. Zargar, J. Javadpour and F. Golestani-Fard, *Mater. Res. Bull.*, 47 (2012) 1494.
11. M. Daroonparvar, M.A.M. Yajid, N.M. Yusof and H.R. Bakhsheshi-Rad, *J. Alloys Compd.*, 688 (2016) 841.
12. Z.P. Yao, P.F. Ju, Q.X. Xia, J.K. Wang, P. Su, H. Wei, D.Q. Li and Z.H. Jiang, *Surf. Coat. Technol.*, 307 (2016) 1236.
13. G. Rapheal, S. Kumar, N. Scharnagl and C. Blawert, *Surf. Coat. Technol.*, 309 (2017) 124.
14. X. Lu, C. Blawert, M.L. Zheludkevich and K.U. Kainer, *Corros. Sci.*, 101 (2015) 201.
15. D.V. Mashtalyar, S.V. Gnedenkov, S.L. Sinebryukhov, I.M. Imshinetskiy and A.V. Puz, *J. Mater. Sci. Technol.*, 33 (2017) 461.
16. S.V. Gnedenkov, S.L. Sinebryukhov, D.V. Mashtalyar, V.S. Egorokin, M.V. Sidorova and A.S. Gnedenkov, *Corros. Sci.*, 85 (2014) 52.
17. H. Nasiri Vatan, R. Ebrahimi-kahrizsangi and M. Kasiti-asgarani, *J. Alloy Compd.*, 683 (2016) 241.
18. X. Lu, M. Schieda, C. Blawert, K.U. Kainer and M.L. Zheludkevich, *Surf. Coat. Technol.*, 307 (2016) 287.
19. D.V. Mashtalyar, S.V. Gnedenkov, S.L. Sinebryukhov, I.M. Imshinetskiy and A.V. Puz, *J. Mater. Sci. Technol.*, 33 (2017) 461.
20. S. Stojadinović, N. Tadić, N. Radić, B. Grbić and R. Vasilić, *Surf. Coat. Technol.*, 310 (2017) 98.
21. T.S. Lim, H.S. Ryu and S.H. Hong, *Corros. Sci.*, 62 (2012) 104.
22. C.S. Kim, M.J. Kim, H. Cho, T. Park and Y. Yun, *Ceramics Int.*, 41 (2015) 12757.
23. X.M. Wang, X.Q. Zeng, G.S. Wu and S.S. Yao, *Appl. Surf. Sci.*, 253 (2006) 2437.
24. L. Eyring, Chapter 27: the binary rare earth oxides, 3 (1979) 337.
25. Z. Shi, M. Liu and A. Atrens, *Corros. Sci.*, 52 (2010) 579.
26. E. McCafferty, *Corros. Sci.*, 47 (2005) 3202.
27. F. Wei, W. Zhang, T. Zhang and F. Wang, *J. Alloys Compd.*, 690 (2017) 195.
28. O. Khaselev, D. Weiss and J. Yahalom, *J. Electrochem. Soc.*, 146 (1999) 1757.
29. L.O. Snizhko, A.L. Yerkohin, A. Pilkington, N.L. Gurevina, D.O. Misnyankina, A. Leyland and A. Matthews, *Electrochim. Acta*, 49 (2004) 2085.
30. M. Laleh, A.S. Rouhaghdam and T. Shahrabi, *J. Alloys Compd.*, 496 (2010) 548.
31. X. Lu, C. Blawert, Y. Huang, H. Ovri, M.L. Zheludkevich and K.U. Kainer, *Acta*, 187 (2016) 20.
32. H. Nasiri Vatan, R.K. Kahrizsangi and M.K. Asgarani, *Tribol. Int.*, 98 (2016) 253.
33. X. Lu, C. Blawert, N.C. Scharnagl and K.U. Kainer, *J. Magnes. Alloys*, 1 (2013) 267.
34. Gh. Barati Darband, M. Aliofkhaezai, P. Hamghalma and N. Valizade, *J. Magnes. Alloys*, 5 (2017) 74.
35. G. Lv, H. Chen, W. Gu, W. Feng, L. Li, E. Niu, X. Zhang and S. Yang, *Curr. Appl. Phys.*, 9 (2009) 324.
36. F. Wei, W. Zhang, T. Zhang and F. Wang, *J. Alloys Compd.*, 690 (2017) 195.
37. X. Zhou, G.E. Thompson, P. Skeldon, G.C. Wood, K. Shimizu and H. Habazaki, *Corros. Sci.*, 41 (1999) 1599.
38. J. Dou, G. Gu and C. Chen, *Mater. Lett.*, 196 (2017) 42.

39. J. Liang, P.B. Srinivasan, C. Blawert, M. Stormer and W. Dietzel, *Electrochim. Acta*, 54 (2009) 3842.
40. R. Arrbral, E. Matykina, F. Viejo, P. Skeldon, G.E. Thompson and M.C. Merino, *Appl. Surf. Sci.*, 254 (2008) 6937.
41. X. Lu, C. Blawert, M.L. Zheludkevich and K.U. Kainer, *Corros. Sci.*, 101 (2015) 201.
42. R. Sprycha, J. Jablonski and E. Matijević, *J. Colloid Interface Sci.*, 149 (1992) 561.
43. X. Cui, Y. Li, Q. Li, G. Jin, M. Ding and F. Wang, *Mater. Chem. Phys.*, 111 (2008) 503.
44. M. Mandal, A.P. Moon, G. Deo, C.L. Mendis and K. Mandal, *Corros. Sci.*, 78 (2014) 172.
45. D. Prasai, J.C. Tuberquia, R.R. Harl, G.K. Jennings and K.I. Bolotin, *ACS Nano*, 6 (2012) 1102.
46. S.V. Lamaka, M.F. Montemor, A.F. Galio, M.L. Zheludkevich, C. Tridade, L.F. Dick and M.G.S. Ferreira, *Electrochim. Acta*, 53 (2008) 4773.
47. H. Ma, D. Li, C. Liu, Z. Huang, D. He, Q. Yan, P. Liu, P. Nash and D. Shen, *Surf. Coat. Technol.*, 266 (2015) 151.
48. M. Ren, S. Cai, T. Liu, K. Huang, X. Wang, H. Zhao, S. Niu, R. Zhang and X. Wu, *J. Alloys Compd.*, 591 (2014) 34.

© 2018 The Authors. Published by ESG (www.electrochemsci.org). This article is an open access article distributed under the terms and conditions of the Creative Commons Attribution license (<http://creativecommons.org/licenses/by/4.0/>).